Microscopic calculation of bremsstrahlung emission in $^3He+\alpha$ collisions

Q. K. K. Liu
Bereich Physik, Hahn-Meitner Institut, D-1000 Berlin 39, Federal Republic of Germany

Y. C. Tang
School of Physics and Astronomy, University of Minnesota, Minneapolis, Minnesota 55455

H. Kanada
Department of Physics, Niigata University, Niigata 950-21, Japan
(Received 19 December 1989)

The bremsstrahlung emission cross section from $^3He+\alpha$ collisions has been calculated and is found to compare quite satisfactorily with the experimental result. To describe the scattering system, we use the single-channel resonating-group wave functions which reproduce the essential characteristics, especially in the energy region including the important ^2F resonances. The photon-emission operator used is translationally invariant and the center-of-mass motion is strictly eliminated from the transition amplitude. The multipole component of this amplitude is written in closed form without invoking the long-wavelength approximation. These formulas can be used immediately for bremsstrahlung emission and other electromagnetic transitions in other light nuclear systems.

I. INTRODUCTION

Electromagnetic (EM) transitions between bound states, besides the eigenvalue spectrum, are important tests of any nuclear-structure model. The microscopic cluster model[1] occupies the strong position of a unified microscopic model of bound and scattering nuclear states in light and light-heavy ions. In light nuclei[2] that have a limited number of bound states, or none at all, bremsstrahlung emission becomes the most important tool as an EM probe of the nuclear models. The reason is that bremsstrahlung emission during nuclear collision is simply an EM transition between nuclear states, albeit both the initial and final states are unbound. In this light, bremsstrahlung gives a key indication of the accuracy of the microscopic cluster model, over and above the predictions of the bound-state energies, positions of the resonances, and off-resonance phase shifts. Semimicroscopic cluster model is often the preferred theory to describe the possible band structure of nuclear-molecular resonances.[3] EM transitions between them are further examples of bremsstrahlung transitions. Experimental confirmation of such collective γ transitions between nuclear-molecular resonances has been sought.[4]

A first application, by Baye and Descouvemont (BD),[5] of the microscopic cluster model to calculate bremsstrahlung is only a recent accomplishment. With their generator-coordinate-method (GCM) formalism they obtained an $\alpha+\alpha$ bremsstrahlung cross section that agreed fairly well with experiment. This was followed up by a macroscopic approach to the same problem by Langanke.[6]

In our present work, we use the microscopic cluster model to investigate bremsstrahlung emission in the $^3He+\alpha$ collision. This is an extension of our previous studies, using the resonating-group-method (RGM) formalism, of EM transitions in the seven-nucleon system.[7-9] In Ref. 7, we examined the charge form factor of ^7Li—an EM transition with a virtual photon. In Refs. 8 and 9, we calculated the electric-dipole radiative capture-reaction $^3He+\alpha\rightarrow{}^7Be+\gamma$—an EM transition between a bound and a scattering state, and the $B(M1)$ and $B(E2)$ values between the ground and first excited states of ^7Li and ^7Be—an EM transition between bound states. We show presently that our bremsstrahlung calculation agrees satisfactorily with the rather sparse experimental result.[10] Hence our complete set of calculations of EM transitions underpins our claim of accuracy for the microscopic cluster model adopted for the system. There is of course room for improvement, which we shall discuss in the later text.

As has been dilated upon elsewhere,[1] in our RGM formalism the Pauli principle is treated exactly and the wave functions used are translationally invariant. In this work the photon-emission operator retains this invariance. These important features should render our results more realistic than those in the literature.[10] In contrast to the transition operators we employed in Refs. 7–9, which are also translationally invariant, we have found a way to be free from the restraint of the long-wavelength approximation altogether. In short, our derivation of the EM transition matrix element is extremely general, insofar as we employed the classical EM operator, dispensing with the long-wavelength approximation, and without any reference to whether the nuclear states involved are bound or not. In this connection, we encompass the treatment of the transition matrix element given in BD.[5] Our expression for the microscopic transition matrix element contains, as a special case, the macroscopic formulas of Ref. 6, where the Pauli principle is only roughly taken into account, thus furnishing it some microscopic basis. To in-

 ©1990 The American Physical Society

clude the effect of the Pauli principle in varying degrees, there exists more modest machinery than the full-blown microscopic model, ranging from the approximated RGM formalism (ARGM),[11] through the orthogonality-condition model (OCM),[3] to the node-counting method.[12] Lately there is also discussion concerning the use of supersymmetric quantum mechanics[13] to generate an entirely phase-equivalent local potential that does not contain any Pauli-forbidden states. The efficacy of these methods has to be measured against the microscopic model via bremsstrahlung and other EM transitions.

Section II is devoted to the derivation of the bremsstrahlung transition matrix element in the RGM formalism and its multipole expansion. The results are given in Sec. III. We present some concluding remarks and comments on other related problems in Sec. IV.

II. FORMULATION

A. Resonating-group wave functions

The RGM formulation of the ^{3}He+α problem has been discussed elsewhere,[14] hence we shall describe only a few salient features relevant to our present work. We adopt, whenever possible, the notation of Ref. 7 (KLT) and Ref. 8 (LKT). In the single-channel approximation, the scattering wave function in the initial channel, labeled by the channel spin $S(=\frac{1}{2})$ and its z component M_{S_i}, has the form [cf. Eqs. (13), (14), and (15) of LKT]

$$\psi^{(+)}_{SM_{S_i}} = \phi^{(+)}_{SM_{S_i}} Z(\mathbf{R}_{\text{c.m.}}) , \tag{1}$$

with

$$\phi^{(+)}_{SM_{S_i}} = \frac{1}{\sqrt{N!}} \mathcal{A} \left[\phi_A \phi_B \left[\frac{1}{R} \sum_{J_i l_i} \sum_{M_i} [4\pi(2l_i+1)]^{1/2} f_{J_i l_i}(R) C(l_i S J_i; 0 M_{S_i} M_i) \mathcal{Y}^{M_i}_{J_i l_i S} \right] \right] , \tag{2}$$

where $\mathcal{A}$ denotes the antisymmetrization operator and $N=7$ is the total number of nucleons. The direction of the incoming momentum is taken to be the z axis. The functions ϕ_A and ϕ_B represent internal functions of the α and ^{3}He clusters, with nuclear charges Z_A and Z_B, respectively. They assume the normalized forms

$$\phi_A = \left[\frac{\alpha_A^3}{4\pi^3} \right]^{3/4} \exp\left[-\tfrac{1}{2}\alpha_A \sum_{i=1}^{4} (\mathbf{r}_i - \mathbf{R}_A)^2 \right] , \tag{3}$$

$$\phi_B = \left[\frac{\alpha_B^2}{3\pi^2} \right]^{3/4} \exp\left[-\tfrac{1}{2}\alpha_B \sum_{i=5}^{7} (\mathbf{r}_i - \mathbf{R}_B)^2 \right] , \tag{4}$$

where $\mathbf{R}_A$ and $\mathbf{R}_B$ are, respectively, the c.m. coordinates of the two clusters. The width parameters are given the values

$$\alpha_A = 0.514 \text{ fm}^{-2} , \tag{5}$$

$$\alpha_B = 0.367 \text{ fm}^{-2} , \tag{6}$$

which reproduce the empirical rms matter radii deduced from electron scattering.[15] In Eq. (2), $C(l_i S J_i; 0 M_{S_i} M_i)$ is the Clebsch-Gordan coefficient in the notation of Rose[16] and $\mathcal{Y}^{M_i}_{J_i l_i S}$ is the spin-isospin-angle function appropriate for $T=\frac{1}{2}$ and $S=\frac{1}{2}$, which has the explicit form

$$\mathcal{Y}^{M_i}_{J_i l_i S} = \sum_{m, M_S} C(l_i S J_i; m M_S M_i) i^{l_i} Y^m_{l_i}(\hat{\mathbf{R}}) \xi^{M_S}_S , \tag{7}$$

where $\mathbf{R}$ is the coordinate vector of the relative distance between the centers of the two clusters. We shall adopt the phase convention $Y^{m*}_l = (-)^m Y^{-m}_l$ for the spherical harmonics. Exploiting the freedom in the choice of the total c.m. motion function $Z(\mathbf{R}_{\text{c.m.}})$, we define

$$Z(\mathbf{R}_{\text{c.m.}}) = \left[\frac{N_A \alpha_A + N_B \alpha_B}{\pi} \right]^{3/4} \times \exp[-\tfrac{1}{2}(N_A \alpha_A + N_B \alpha_B) \mathbf{R}^2_{\text{c.m.}}] , \tag{8}$$

with $N_A=4$ and $N_B=3$ being the nucleon numbers of the α and ^{3}He clusters, respectively. This facilitates the computation of matrix elements in which clusters of unequal widths are involved, when used in conjunction with the complex-generator-coordinate technique (CGC).[17] We shall show in Sec. II D that this choice of $Z(\mathbf{R}_{\text{c.m.}})$ is also tailor-made for the handling of translational invariance of the transition matrix elements. The relative-motion function $f_{J_i l_i}(R)$ is the variational solution of the RGM formalism.[1] Outside the region of the nuclear interaction, it is normalized to the Coulomb-distorted wave of unit current, i.e.,

$$f_{J_i l_i}(R) = \frac{1}{k_i} \exp[i(\sigma_{l_i} + \delta_{J_i l_i})][F_{l_i}(\eta_i, k_i R)\cos\delta_{J_i l_i} + G_{l_i}(\eta_i, k_i R)\sin\delta_{J_i l_i}] \tag{9}$$

where η_i is the Coulomb parameter and k_i the asymptotic wave number in the initial channel. Here, F_{l_i}, G_{l_i}, and σ_{l_i} are, respectively, the regular Coulomb function, the irregular Coulomb function and the Coulomb phase shift of the l_ith partial wave, and $\sigma_{J_i l_i}$ is the nuclear phase shift in the $(J_i l_i)$ partial-wave channel. A detailed discussion of the solution $f_{J_i l_i}(R)$ can be found in Ref. 1.

The partial-wave expansion of the outgoing wave is similarly defined as in Eq. (1),

$$\psi^{(-)}_{SM_{S_f}} = \phi^{(-)}_{SM_{S_f}} Z(\mathbf{R}_{\text{c.m.}}) , \tag{10}$$

with

$$\phi^{(-)}_{SM_{S_f}} = \frac{1}{\sqrt{N!}}\mathcal{A}\left[\phi_A\phi_B\left[\frac{1}{R}\sum_{J_f l_f}\sum_{M_f} 4\pi C(l_f S J_f; m_f M_{S_f} M_f) f^*_{J_f l_f}(R)\mathcal{Y}^{M_f}_{J_f l_f S} Y^{m_f *}_{l_f}(\hat{\mathbf{k}}_f)\right]\right], \tag{11}$$

where

$$\mathcal{Y}^{M_f}_{J_f l_f S} = \sum_{m', M'_S} C(l_f S J_f; m' M'_S M_f) i^{l_f} Y^{m'}_{l_f}(\hat{\mathbf{R}}) \xi^{M'_S}_S . \tag{12}$$

For large R, the relative-motion function in the final channel $f_{J_f l_f}(R)$ has the same form as in Eq. (9) with the label i replaced by f.

B. Brief discussion of the resonating-group parameters and scattering results

In the present investigation, we focus our attention on the low-energy scattering states of ^{3}He+α. In this energy region, the spectrum is dominated by the $\frac{7}{2}^-$ (2.98 MeV, Γ=175 keV) and $\frac{5}{2}^-$ (5.14 MeV, Γ=1.2 MeV) resonances, and a second $\frac{5}{2}^-$ resonance at 5.62 MeV.[2] The two lower resonances are amenable to the straightforward interpretation of F-wave resonances between the ^{3}He and α clusters.[14] We take this into account in the choice of parameters for the nucleon-nucleon potential. The nucleon-nucleon potential we adopt is that of KLT and LKT.[7,8] These potentials have minor differences in their parameters because they were fine-tuned to reproduce the bound states of ^{7}Li and ^{7}Be, respectively. For the scattering phenomenon at hand, we use parameters that reproduce the two F-wave resonances at the experimental energies, i.e.,

$$\begin{aligned} u &= 0.996 , \\ V_\lambda &= -73.53 \text{ MeV} , \\ V_{\lambda\tau} &= 398.61 \text{ MeV} . \end{aligned} \tag{13}$$

The other $\frac{5}{2}^-$ resonance at 5.62 MeV has mainly a $p+^6$Li configuration that we can neglect without a great loss of accuracy in the present instance. We summarize in Table I the phase shifts at selected energies for partial waves up to l=4. We use the notation δ_l^+ and δ_l^- for phase shifts in the channels with $J=l+\frac{1}{2}$ and $J=l-\frac{1}{2}$, respectively. In Fig. 1, we show a comparison of the experimental phase shifts around the $\frac{7}{2}^-$ and $\frac{5}{2}^-$ resonances with the theoretical predictions. The sharp $\frac{7}{2}^-$ resonance and its width are very accurately reproduced and the prediction for the $\frac{5}{2}^-$ resonance is also quite satisfactory.

C. The bremsstrahlung cross section

The kinematics of three particles in the final channel of a nuclear reaction often requires special attention.[18] The kinematics is completely determined when five independent observables are measured experimentally, because four of the nine coordinates associated with the three outgoing particles are not independent due to the conservation of momenta and total energy. We can use the α, ^{3}He, and the photon as an example in this discussion. In a theoretical calculation, quantities are expressed in the c.m. system in which the five convenient observables may be the direction $\Omega_f=(\theta_f,\phi_f)$ of the relative momentum between α and ^{3}He, the direction $\Omega_\gamma=(\theta_\gamma,\phi_\gamma)$ of the emitted photon relative to the total c.m. of α and ^{3}He, and the energy E_γ of the photon. However, the measured quantities are in the laboratory system in which the convenient observables may be the directions $\Omega_A=(\theta_A,\phi_A)$ and $\Omega_B=(\theta_B,\phi_B)$ of α and ^{3}He, respectively, and the polar angle θ_γ of the photon. The theoretical cross section expressed in a set of c.m. observables can be transformed to a set of laboratory observables by the multiplication of the appropriate Jacobian.

The available experimental result[10] was measured in the Harvard geometry in which the incident projectile, the α and ^{3}He clusters in the final channel are in a plane, i.e., ϕ_A, ϕ_B, and ϕ_γ are equal to 0 or π, and the α and ^{3}He scatter symmetrically with respect to the direction of the incident particle, i.e., $\theta_A=\theta_B$. A thorough discussion of this kinematic arrangement is given in Refs. 5 and 19. The coplanar laboratory cross section, calculated to the first-order distorted-wave approximation, is given by[5]

TABLE I. ^{3}He+α phase shifts (in deg) as a function of E (MeV).

E	δ_0	δ_1^+	δ_1^-	δ_2^+	δ_2^-	δ_3^+	δ_3^-	δ_4^+	δ_4^-
1.16	−8.99	−6.38	−9.15	−0.13	−0.15	0.09	0.06	−0.001	−0.001
1.90	−19.24	−15.69	−20.87	−0.55	−0.64	1.07	0.58	−0.008	−0.008
2.51	−26.59	−23.26	−29.86	−0.98	−1.21	6.54	1.99	−0.029	−0.030
2.83	−29.94	−26.91	−34.09	−1.18	−1.52	27.24	3.37	−0.048	−0.049
2.98	−31.45	−28.61	−36.03	−1.27	−1.66	89.97	4.28	−0.060	−0.062
3.30	−34.50	−32.07	−39.97	−1.41	−1.94	159.01	6.94	−0.090	−0.093
4.23	−42.28	−41.15	−50.08	−1.42	−2.52	169.30	26.87	−0.222	−0.232
4.57	−44.88	−44.22	−53.44	−1.26	−2.62	169.94	45.00	−0.287	−0.301
5.14	−49.01	−49.06	−58.67	−0.78	−2.66	170.48	89.66	−0.408	−0.433
6.00	−54.82	−55.74	−65.79	0.36	−2.44	170.93	126.80	−0.605	−0.654
8.00	−67.15	−69.24	−79.87	3.97	−1.35	171.78	143.49	−0.904	−1.084
12.05	−88.03	−90.77	−101.68	8.53	−1.19	172.87	147.59	1.030	−0.091

$$\frac{d^3\sigma}{d\Omega_A d\Omega_B d\theta_\gamma} = \frac{1}{(2\pi\hbar)^4\hbar} p_B^4 v_f \frac{\sin^2\theta_A \sin^2\theta_B}{\sin^5(\theta_A+\theta_B)} \times \tfrac{1}{2} \sum_{\mu, M_{S_i}} |\langle \phi^{(-)}_{SM_{S_f}} | \tilde{H}_e(\mathbf{k}_\gamma, \boldsymbol{\varepsilon}^*_\mu) | \phi^{(+)}_{SM_{S_i}} \rangle|^2 , \tag{14}$$

where $\mathbf{p}_B$ is the momentum of the incident particle and $\mathbf{v}_f$ is the final relative velocity between the ^{3}He and α in the c.m. system. $\tilde{H}_e$ is the translationally invariant photon-emission operator, with photon wave vector $\mathbf{k}_\gamma$ and circular polarization $\boldsymbol{\varepsilon}^*_\mu$.[20] A more detailed discussion of this operator will be given in the next section. The factor $\frac{1}{2}$ in front of the summation sign is due to the averaging over the initial spin component M_{S_i}.

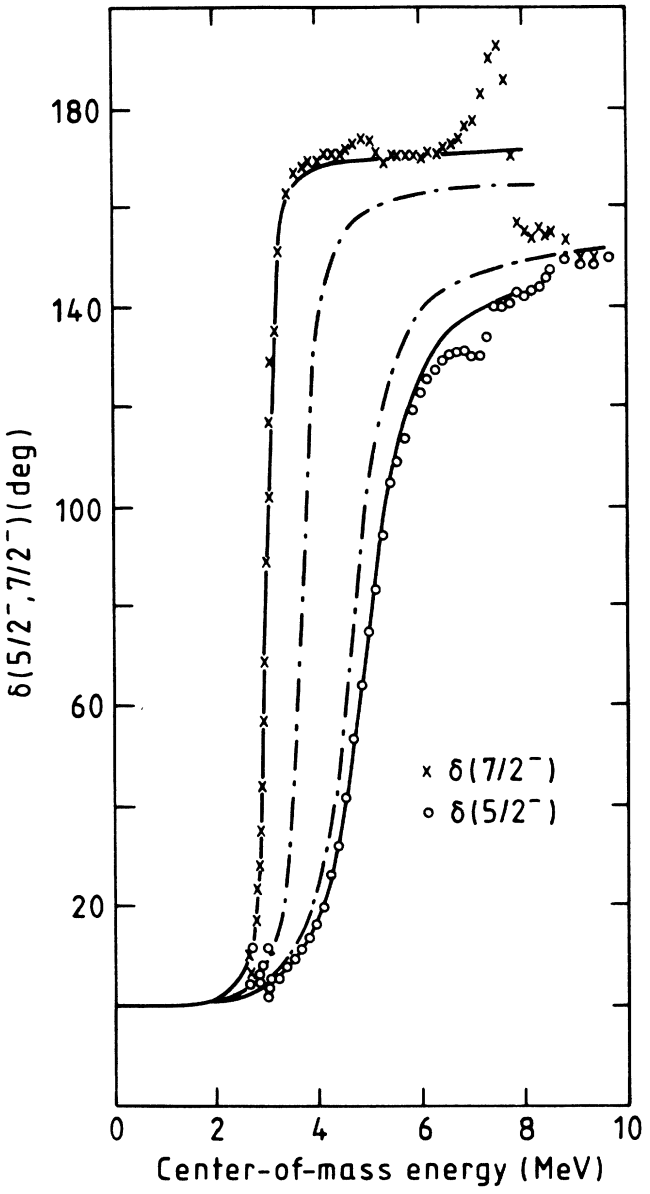

FIG. 1. Comparison of empirical data with the calculated $\delta(\frac{7}{2}^-)$ and $\delta(\frac{5}{2}^-)$ phase shifts as a function of energy in the ^{3}He+α system. The empirical data are taken from Ref. 14. The dot-dash lines (—·—·—·) are calculated with the LKT (Ref. 8) parameters. The solid lines (——) are calculated with the readjusted parameters of the present work to better reproduce the positions of the $\frac{7}{2}^-$ and $\frac{5}{2}^-$ resonances.

The following equations are required in order to convert quantities in the c.m. system to the laboratory system:

$$E_f = E_i - E_\gamma , \tag{15}$$

$$E_\gamma = \left[\frac{p_B^2}{2N_B m_n} \right] \left[1 - \frac{N_A \sin^2\theta_A + N_B \sin^2\theta_B}{N_A \sin^2(\theta_A+\theta_B)} \right] , \tag{16}$$

$$\cot\theta_f = \frac{N_A \cot\theta_B - N_B \cot\theta_A}{N} , \tag{17}$$

$$\phi_f = 0 . \tag{18}$$

In these equations, E_i and E_f are the asymptotic kinetic energies between ^{3}He and α in the initial and final channels in the c.m. system. N_B refers to the incident cluster and m_n is the nucleon mass.

D. Elimination of the c.m. motion in the transition matrix element

According to Refs. 20 and 21, the spin-independent photon-emission operator is given by the symmetrized interaction of the nucleon charge currents with the photon vector potentials $\mathbf{A}$, written now in terms of the translationally invariant coordinates of the nucleons $\boldsymbol{\rho}_i$ as

$$\tilde{H}_e(\mathbf{k}_\gamma, \boldsymbol{\varepsilon}^*_\mu) = -\sum_{i=1}^{N} \frac{e}{m_n c} g_l(i) \frac{\mathbf{P}^*_i \cdot \mathbf{A}^*(\boldsymbol{\rho}_i) + \mathbf{A}^*(\boldsymbol{\rho}_i) \cdot \mathbf{P}^*_i}{2} , \tag{19}$$

where e is the proton charge and g_l is 0 or 1 for neutron or proton, respectively. Given a set of N nucleon-coordinates $(\mathbf{r}_1, \ldots, \mathbf{r}_N)$, which refer to an arbitrary origin, we obtain the following set of N translationally invariant coordinates in a straightforward manner:

$$\begin{aligned} \boldsymbol{\rho}_i &= \mathbf{r}_i - \mathbf{R}_{\text{c.m.}}, \quad (i = 1 \text{ to } N-1) , \\ \mathbf{R}_{\text{c.m.}} &= \frac{\mathbf{r}_1 + \cdots + \mathbf{r}_N}{N} . \end{aligned} \tag{20}$$

The corresponding momenta are

$$\begin{aligned} \mathbf{P}_i &= \mathbf{p}_i - \frac{\mathbf{P}_{\text{c.m.}}}{N}, \quad (i = 1 \text{ to } N-1) , \\ \mathbf{P}_{\text{c.m.}} &= \mathbf{p}_1 + \cdots + \mathbf{p}_N . \end{aligned} \tag{21}$$

The momentum operator of the ith nucleon is $\mathbf{P}^*_i = i\hbar\nabla_{\boldsymbol{\rho}_i}$. The vector potential,

$$\mathbf{A}^*(\boldsymbol{\rho}_i) = \boldsymbol{\varepsilon}^*_\mu \exp(-i\mathbf{k}_\gamma \cdot \boldsymbol{\rho}_i) , \tag{22}$$

satisfies the transverse gauge condition,

$$\nabla_{\boldsymbol{\rho}_i} \cdot \mathbf{A}^*(\boldsymbol{\rho}_i) = 0 , \tag{23}$$

implying that $\boldsymbol{\varepsilon}^*_\mu \cdot \mathbf{k}_\gamma = 0$.

We neglect the spin-dependent emission operator in this study because there is strong evidence that its contribution to the bremsstrahlung emission is small.[22] We offer a further remark on this later in this section.

To calculate the transition matrix element for the cross section in Eq. (14), we first consider the emission operator written in terms of the nucleon-coordinates $\mathbf{r}_i$,

$$H_e(\mathbf{k}_\gamma,\boldsymbol{\varepsilon}_\mu^*)=-\sum_{i=1}^{N}\frac{e}{m_n c}g_l(i)\boldsymbol{\varepsilon}_\mu^*\exp(-i\mathbf{k}_\gamma\cdot\mathbf{r}_i)\cdot\mathbf{p}_i^* \ . \tag{24}$$

Substituting the inverses of Eqs. (20) and (21) into Eq. (24), we obtain

$$H_e=\tilde{H}_e\exp(-i\mathbf{k}_\gamma\cdot\mathbf{R}_{\text{c.m.}})-\sum_{i=1}^{N}\frac{e}{Nm_n c}g_l(i)\boldsymbol{\varepsilon}_\mu^*\exp(-i\mathbf{k}_\gamma\cdot\boldsymbol{\rho}_i)\cdot\exp(-i\mathbf{k}_\gamma\cdot\mathbf{R}_{\text{c.m.}})\mathbf{P}_{\text{c.m.}}^* \ , \tag{25}$$

which has the attractive feature that in each of the two terms the c.m. coordinate is separated out from the other independent variables. If the ansatz for the many-body wave function also has this separability,

$$\psi_j(\mathbf{r}_1,\ldots,\mathbf{r}_N)=\phi_j(\boldsymbol{\rho}_1,\ldots,\boldsymbol{\rho}_{N-1})Z(\mathbf{R}_{\text{c.m.}}) \ , \tag{26}$$

then the matrix element of H_e takes on the form

$$\langle\psi_j|H_e|\psi_k\rangle=\langle\phi_j|\tilde{H}_e|\phi_k\rangle\langle Z|\exp(-i\mathbf{k}_\gamma\cdot\mathbf{R}_{\text{c.m.}})|Z\rangle$$
$$-\langle\phi_j|\sum_{i=1}^{N}\frac{e}{Nm_n c}g_l(i)\exp(-i\mathbf{k}_\gamma\cdot\boldsymbol{\rho}_i)|\phi_k\rangle\boldsymbol{\varepsilon}_\mu^*\cdot\langle Z|\exp(-i\mathbf{k}_\gamma\cdot\mathbf{R}_{\text{c.m.}})\mathbf{P}_{\text{c.m.}}^*|Z\rangle \ . \tag{27}$$

Our RGM wave functions, Eqs. (1), (2), (10), and (11), do have this separability property. In the second term of Eq. (27), if we let the operator $\mathbf{P}_{\text{c.m.}}^*$ operate to the left, and make use of the fact that $Z(\mathbf{R}_{\text{c.m.}})$ of Eq. (8) is a real function that vanishes at large $R_{\text{c.m.}}$, it is easy to see that the part

$$\langle Z|\exp(-i\mathbf{k}_\gamma\cdot\mathbf{R}_{\text{c.m.}})\mathbf{P}_{\text{c.m.}}^*|Z\rangle$$
$$=-\tfrac{1}{2}\hbar\mathbf{k}_\gamma\langle Z|\exp(-i\mathbf{k}_\gamma\cdot\mathbf{R}_{\text{c.m.}})|Z\rangle \ . \tag{28}$$

Then the transverse gauge condition, $\boldsymbol{\varepsilon}_\mu^*\cdot\mathbf{k}_\gamma=0$, ensures that the second term of Eq. (27) vanishes. Introducing $\psi_{SM_{S_i}}^{(+)}$, $\phi_{SM_{S_i}}^{(+)}$, $\psi_{SM_{S_f}}^{(-)}$, and $\phi_{SM_{S_f}}^{(-)}$ where appropriate, we reduce Eq. (27), after slight rearrangement, to

$$\langle\phi_{SM_{S_f}}^{(-)}|\tilde{H}_e|\phi_{SM_{S_i}}^{(+)}\rangle=\frac{\langle\psi_{SM_{S_f}}^{(-)}|H_e|\psi_{SM_{S_i}}^{(+)}\rangle}{F_{\text{c.m.}}} \ , \tag{29}$$

where, after inserting the explicit form of $Z(\mathbf{R}_{\text{c.m.}})$ from Eq. (8), we have

$$F_{\text{c.m.}}=\langle Z|\exp(-i\mathbf{k}_\gamma\cdot\mathbf{R}_{\text{c.m.}})|Z\rangle$$
$$=\exp\left[-\frac{k_\gamma^2}{4(N_A\alpha_A+N_B\alpha_B)}\right] \ . \tag{30}$$

The important result of this section is contained in Eqs. (29) and (30), which show that the translationally invariant matrix element of the emission operator can be expressed in terms of matrix element referred to an arbitrary origin divided by a simple algebraic factor. Although the sufficient condition to obtain the form of EM transition matrix element of Eq. (29) is merely the reality and normalizability of the c.m. function $Z(\mathbf{R}_{\text{c.m.}})$, in practice we take advantage of the CGC technique, especially useful when the oscillator widths are unequal ($\alpha_A\neq\alpha_B$), and assume the explicit form of Eq. (8) for $Z(\mathbf{R}_{\text{c.m.}})$, which transforms the numerator on the right-hand side of Eq. (29) into a matrix element between antisymmetrized products of single-particle functions of the variables $(\mathbf{r}_1,\ldots,\mathbf{r}_N)$.[17,7-9] We are of course familiar with this useful form of EM transition matrix element. It appeared in our calculations for the form factor (KLT) and the radiative capture reaction (LKT). With $\alpha_A=\alpha_B$, it also made its first appearance in an oscillator shell model calculation of form factors.[23] We must stress that the correction factor in Eq. (29) is derived before a multipole expansion of the operator is made. Hence an expansion of the photon-emission operator in Eq. (29) into multipoles automatically gives us translationally invariant electric- and magnetic-multipole transition matrix elements. We achieve this without resorting to any long-wavelength approximation.[8,5,24,25] With hardly any extra effort, we show in Appendix A that the form of Eq. (29) is also valid for the spin-dependent term of the photon-emission operator.[20,21]

Discussion of the photon-emission operator in the standard texts[26] emphasizes the difficulty engendered when one tries to remove the c.m. motion, excepting the case of electric-dipole in the long-wavelength approximation. We offer our treatment of the c.m. motion as a notable, constructive contribution to the discussion of EM transition in nuclear many-body theory. We show in the next section that this leads to "closed" expressions for the matrix element.

Other wave functions with the separability *ansatz* of Eq. (26) would find Eq. (27) immediately applicable, and if the choice of c.m. motion function were such that the transverse gauge condition, $\boldsymbol{\varepsilon}_\mu^*\cdot\mathbf{k}_\gamma=0$, could be brought to bear, then the convenient form of Eq. (29) would result. An obvious example of this is the cluster wavefunction in the GCM formalism, with equal oscillator widths ($\alpha_A=\alpha_B$). Then, the numerator of Eq. (29) could be calculated in GCM, if so desired. From this point of view, our derivation of the transition matrix element in the following sections contains the work of BD as a special case. Another useful example is the shell model in the oscillator basis in which the c.m. motion can be de-

scribed by an oscillator function. For the rest of this paper, we shall refer to the numerator on the right-hand side of Eq. (29) as the independent-particle transition matrix element in contrast to the left-hand side of Eq. (29), which is the translationally invariant transition matrix element.

E. The transition matrix element

It is useful to extract from Eqs. (2) and (7), for the initial channel, a new function

$$G_i(\mathbf{R}')=\frac{f_{J_i l_i}(R')}{R'}Y_{l_i}^{m}(\hat{\mathbf{R}}')\ , \tag{31}$$

and similarly for the final channel

$$G_f(\mathbf{R}')=\frac{f^*_{J_f l_f}(R')}{R'}Y_{l_f}^{m'}(\hat{\mathbf{R}}')\ . \tag{32}$$

We use these functions to calculate the transition matrix element, in independent particles coordinates, of the photon-emission operator of Eq. (24), using the CGC technique,[7,8]

$$\frac{1}{\sqrt{N!}}\langle\phi_A\phi_B G_f(\mathbf{R}')Z(\mathbf{R}_{\text{c.m.}})|H_e(\mathbf{k}_\gamma,\boldsymbol{\varepsilon}^*_\mu)|\mathcal{A}\{\phi_A\phi_B G_i(\mathbf{R}')\}Z(\mathbf{R}_{\text{c.m.}})\rangle$$

$$=Z_A F_0^b+Z_B F_0^c+4(F_1^b+F_1^c)+2(F_1^{a1}+F_1^{a2})+2(F_2^b+F_2^c)+4(F_2^{a1}+F_2^{a2})+2(F_3^{a1}+F_3^{a2})\ . \tag{33}$$

The superscripts of the F functions denote the interaction types and the subscripts label the direct and exchange terms, e.g., 0 for direct terms and 1 for one-nucleon-exchange terms between the two clusters, and so on.[7,8] The explicit expressions for the F function are given below.

(i) The b-type direct term $Z_A F_0^b$ is given by

$$Z_A F_0^b=\exp(-\mu_{b0}k_\gamma^2)\int G_f^*(\mathbf{R}')\left[-\frac{Z_A e}{N_A m_n c}\boldsymbol{\varepsilon}^*_\mu\exp(-i\mathbf{k}_\gamma\cdot\gamma_b\mathbf{R}')\cdot\frac{\hbar}{-i}\nabla_{\mathbf{R}'}\right]G_i(\mathbf{R}')d\mathbf{R}'\ . \tag{34}$$

(ii) the c-type direct term $Z_B F_0^c$ is given by

$$Z_B F_0^c=-\exp(-\mu_{c0}k_\gamma^2)\int G_f^*(\mathbf{R}')\left[-\frac{Z_B e}{N_B m_n c}\boldsymbol{\varepsilon}^*_\mu\exp(-i\mathbf{k}_\gamma\cdot\gamma_c\mathbf{R}')\cdot\frac{\hbar}{-i}\nabla_{\mathbf{R}'}\right]G_i(\mathbf{R}')d\mathbf{R}'\ . \tag{35}$$

The quantities μ_{b0}, μ_{c0}, γ_b, and γ_c are defined in Eqs. (58) and (64) of KLT and Eqs. (41) and (43) of LKT, respectively.

(iii) The b-type exchange term F_x^b, with $x=1,2$, is

$$F_x^b=E_x^b\int G_f^*(\mathbf{R}')\frac{\mathbf{R}''-\mathbf{R}'}{i}\cdot\frac{e\hbar}{m_n c}\boldsymbol{\varepsilon}^*_\mu I_x^b(\mathbf{R}',\mathbf{R}'')G_i(\mathbf{R}'')d\mathbf{R}'d\mathbf{R}''\ . \tag{36}$$

(iv) The c-type exchange term F_x^c, with $x=1,2$, is

$$F_x^c=E_x^c\int G_f^*(\mathbf{R}')\frac{\mathbf{R}''-\mathbf{R}'}{i}\cdot\frac{e\hbar}{m_n c}\boldsymbol{\varepsilon}^*_\mu I_x^c(\mathbf{R}',\mathbf{R}'')G_i(\mathbf{R}'')d\mathbf{R}'d\mathbf{R}''\ . \tag{37}$$

(v) The $a1$-type exchange term F_x^{a1}, with $x=1,2,3$, is

$$F_x^{a1}=\int G_f^*(\mathbf{R}')\frac{P_x^a\mathbf{R}''-Q_x^a\mathbf{R}'}{i}\cdot\frac{e\hbar}{m_n c}\boldsymbol{\varepsilon}^*_\mu I_x^{a1}(\mathbf{R}',\mathbf{R}'')G_i(\mathbf{R}'')d\mathbf{R}'d\mathbf{R}''\ . \tag{38}$$

(vi) The $a2$-type exchange term F_x^{a2}, with $x=1,2,3$, is

$$F_x^{a2}=\int G_f^*(\mathbf{R}')\frac{Q_x^a\mathbf{R}''-P_x^a\mathbf{R}'}{i}\cdot\frac{e\hbar}{m_n c}\boldsymbol{\varepsilon}^*_\mu I_x^{a2}(\mathbf{R}',\mathbf{R}'')G_i(\mathbf{R}'')d\mathbf{R}'d\mathbf{R}''\ , \tag{39}$$

where $I_x^b(\mathbf{R}',\mathbf{R}'')$, $I_x^c(\mathbf{R}',\mathbf{R}'')$, $I_x^{a1}(\mathbf{R}',\mathbf{R}'')$, and $I_x^{a2}(\mathbf{R}',\mathbf{R}'')$ are defined in Eqs. (60), (66), (47), and (56) of KLT, with $\mathbf{q}$ substituted by $\mathbf{k}_\gamma$. The coefficients E_x^b, E_x^c, P_x^a, and Q_x^a are

$$E_x^b=\frac{\mu_0}{2x}\gamma_b\left[\left(1+\frac{x}{N_B}\right)\alpha_A+\left(1-\frac{x}{N_B}\right)\alpha_B\right]\ , \tag{40}$$

$$E_x^c=\frac{\mu_0}{2x}\gamma_c\left[\left(1-\frac{x}{N_A}\right)\alpha_A+\left(1+\frac{x}{N_A}\right)\alpha_B\right]\ , \tag{41}$$

$$P_x^a=-\frac{1}{2x\Gamma_x}[(\alpha_A+\alpha_B)(N_A\alpha_A+N_B\alpha_B)\lambda_{ax}x^2+\mu_0(N_B\alpha_B^2-N_A\alpha_A^2+N\alpha_A\alpha_B)x+\mu_0^2(\alpha_A+\alpha_B)(N_A\alpha_A-N_B\alpha_B)]\ , \tag{42}$$

$$Q_x^a=-\frac{1}{2x\Gamma_x}[(\alpha_A+\alpha_B)(N_A\alpha_A+N_B\alpha_B)\lambda_{ax}x^2+\mu_0(N_B\alpha_B^2-N_A\alpha_A^2-N\alpha_A\alpha_B)x+\mu_0^2(\alpha_A+\alpha_B)(N_A\alpha_A-N_B\alpha_B)] , \tag{43}$$

where μ_0, Γ_x, and λ_{ax} are defined in Eqs. (42), (51), and (41) of KLT. The tedium of deriving algebraically the "closed" expressions of Eqs. (34)–(43) from Eq. (33) was greatly lightened by the use of MACSYMA (Ref. 27) on a SYMBOLICS processor.

The reason for defining the functions $G_i(\mathbf{R}')$ and $G_f(\mathbf{R}')$ is now apparent on examining Eqs. (34)–(39). Unencumbered by unnecessary Clebsch-Gordan coefficients, we see the general applicability of these equations without reference to whether the functions $G_i(\mathbf{R}')$ and $G_f(\mathbf{R}')$ are bound or unbound. We postpone further discussion of the physical interpretation of the equations until Sec. II G.

F. The multipole expansion

The multipole components of the transition matrix element can be obtained by the multipole expansion of the photon-emission operators pertaining to each individual nucleon coordinate in Eq. (24). However, the application of the CGC technique enables us to make instead the multipole expansion in Eqs. (34)–(39), for which the subsequent algebra is much more tractable.

For the b-type direct term of Eq. (34), we expand[28]

$$\boldsymbol{\varepsilon}_\mu^*\exp(-i\gamma_b\mathbf{k}_\gamma\cdot\mathbf{R}')=-\sum_\sigma\sum_{L,M}\sqrt{2\pi(2L+1)}(-i)^L\mu^\sigma\,\mathbf{A}_{LM}^{\sigma *}(\gamma_b\mathbf{k}_\gamma,\mathbf{R}')\mathcal{D}_{M\mu}^{L*}(\hat{\mathbf{R}}_\gamma) , \tag{44}$$

where $\sigma=0$ and 1 for electric- and magnetic-multipole, respectively, and (L,M) are the multipolarity and its z component. The rotation matrix $\mathcal{D}_{M\mu}^{L*}$ depends on the Euler angles $\hat{\mathbf{R}}_\gamma=(-\phi_\gamma,-\theta_\gamma,0)$. Explicitly, the electric ($\sigma=0$) component is

$$\mathbf{A}_{LM}^{\sigma=0}(\gamma_b\mathbf{k}_\gamma,\mathbf{R}')=\frac{1}{\gamma_b k_\gamma\sqrt{L(L+1)}}\nabla\times\mathbf{L}[j_L(\gamma_b k_\gamma R')Y_L^M(\hat{\mathbf{R}}')] , \tag{45}$$

and the magnetic ($\sigma=1$) component is

$$\mathbf{A}_{LM}^{\sigma=1}(\gamma_b\mathbf{k}_\gamma,\mathbf{R}')=\frac{1}{\sqrt{L(L+1)}}\mathbf{L}[j_L(\gamma_b k_\gamma R')Y_L^M(\hat{\mathbf{R}}')] , \tag{46}$$

where j_L is the spherical Bessel function.[29]

For the c-type direct term of Eq. (35), we can use Eqs. (44)–(46) again, with γ_c substituting for γ_b.

For the exchange terms, we need the expansion

$$\frac{\mathbf{R}'}{i}\cdot\boldsymbol{\varepsilon}_\mu^*\exp(-i\zeta\mathbf{k}_\gamma\cdot\mathbf{R}')=-\frac{1}{\zeta k_\gamma}\sum_{l_\beta m_\beta}(-i)^{l_\beta}\sqrt{2\pi l_\beta(l_\beta+1)(2l_\beta+1)}j_{l_\beta}(\zeta k_\gamma R')Y_{l_\beta}^{m_\beta}(\hat{\mathbf{R}}')\mathcal{D}_{m_\beta-\mu}^{l_\beta}(\hat{\mathbf{R}}_\gamma) , \tag{47}$$

where ζ stands for a coefficient that is defined differently for the functions $I_x^b(\mathbf{R}',\mathbf{R}'')$, $I_x^c(\mathbf{R}',\mathbf{R}'')$, $I_x^{a1}(\mathbf{R}',\mathbf{R}'')$, and $I_x^{a2}(\mathbf{R}',\mathbf{R}'')$. Their explicit definitions are in Eqs. (42), (44), (36), (37), (38), and (39) of LKT.

We can now develop a multipole expansion of Eqs. (34)–(39) by making use of Eqs. (44)–(47) wherever applicable. Combining Eq. (33) with Eqs. (2) and (11), we arrive at the multipole expansion of the independent-particle transition matrix element of Eq. (29),

$$\langle\psi_{SM_{S_f}}^{(-)}|H_e|\psi_{SM_{S_i}}^{(+)}\rangle=\sum_\sigma\sum_{LM}\sum_{J_i l_i}\sum_{J_f l_f}\sum_{M_i M_f}C(l_iSJ_i;0M_{S_i}M_i)C(l_fSJ_f;m_fM_{S_f}M_f)C(J_iLJ_f;M_iMM_f)$$
$$\times X_L^\sigma(J_il_iJ_fl_f)Y_{l_f}^{m_f}(\hat{\mathbf{k}}_f)\mathcal{D}_{M\mu}^{L*}(\hat{\mathbf{R}}_\gamma) , \tag{48}$$

where

$$X_L^\sigma(J_il_iJ_fl_f)=4\pi\sqrt{4\pi(2l_i+1)}\tilde{X}_L^\sigma(J_il_iJ_fl_f) , \tag{49}$$

in which the reduced matrix element $\tilde{X}_L^\sigma(J_il_iJ_fl_f)$ can be broken down into direct and exchange terms and different interaction types as is done in Eq. (33),

$$\tilde{X}_L^\sigma(J_il_iJ_fl_f)=Z_A\tilde{X}_0^b+Z_B\tilde{X}_0^c+4(\tilde{X}_1^b+\tilde{X}_1^c)+2(\tilde{X}_1^{a1}+\tilde{X}_1^{a2})+2(\tilde{X}_2^b+\tilde{X}_2^c)+4(\tilde{X}_2^{a1}+\tilde{X}_2^{a2})+2(\tilde{X}_3^{a1}+\tilde{X}_3^{a2}) . \tag{50}$$

For electric multipoles ($\sigma=0$), the direct terms are

$$Z_A\tilde{X}_0^b=a(J_il_iJ_fl_f;LS)C(l_iLl_f;000)i^L\sqrt{2\pi L(L+1)(2L+1)}\left[-\frac{Z_Ae\hbar}{N_Am_nc}\right]\frac{\tilde{I}_0^b}{\gamma_bk_\gamma}\exp(-\mu_{b0}k_\gamma^2) , \tag{51}$$

$$Z_B\tilde{X}^{\,c}_0=a(J_il_iJ_fl_f;LS)C(l_iLl_f;000)i^L\sqrt{2\pi L(L+1)(2L+1)}\left[\frac{Z_Be\hbar}{N_Bm_nc}\right]\frac{\tilde{I}^{\,c}_0}{\gamma_ck_\gamma}\exp(-\mu_{c0}k_\gamma^2)\ , \tag{52}$$

where the coefficient $a(J_il_iJ_fl_f;LS)$ is

$$a(J_il_iJ_fl_f;LS)=i^{l_i-l_f}(-1)^{l_i+2l_f+S-J_f}\left[\frac{(2J_i+1)(2l_i+1)(2L+1)}{4\pi}\right]^{1/2}W(l_il_fJ_iJ_f;LS)\ , \tag{53}$$

and the radial integral $\tilde{I}^{\,b}_0$ is[22]

$$\tilde{I}^{\,b}_0=\int f_{J_fl_f}(R')j_L(\gamma_bk_\gamma R')\frac{d}{dR'}\left[\frac{f_{J_il_i}(R')}{R'}\right]dR'$$
$$-\frac{1}{2L(L+1)}[l_f(l_f+1)-L(L+1)-l_i(l_i+1)]\int\frac{f_{J_fl_f}(R')}{R'}\frac{d}{dR'}[R'j_L(\gamma_bk_\gamma R')]\frac{f_{J_il_i}(R')}{R'}dR'\ . \tag{54}$$

The radial integral $\tilde{I}^{\,c}_0$ is similarly defined as Eq. (54) with γ_b replaced by γ_c. The exchange terms have the general form

$$\tilde{X}_x^{\text{type}}=a(J_il_iJ_fl_f;LS)T_x\frac{e\hbar}{m_nc}\exp(-\mu_xk_\gamma^2)$$
$$\times\sum_{l_\alpha l_\beta l}\sqrt{2\pi(2l+1)}i^{l_\alpha+l_\beta}(2l_\alpha+1)(2l_\beta+1)C(l_il_\beta l;000)C(ll_\alpha l_f;000)W(l_il_\beta l_fl_\alpha;lL)$$
$$\times\left[U_x\frac{\sqrt{l_\beta(l_\beta+1)}}{\tilde{\beta}k_\gamma}C(l_\alpha l_\beta L;0-\mu-\mu)-V_x\frac{\sqrt{l_\alpha(l_\alpha+1)}}{\tilde{\alpha}k_\gamma}C(l_\alpha l_\beta L;-\mu 0-\mu)\right]\tilde{I}_x^{\text{type}}\ . \tag{55}$$

The coefficient T_x is defined in Eq. (33) of LKT. The exchange radial integral has the general form

$$\tilde{I}_x^{\text{type}}=\int f_{J_fl_f}(R')j_{l_\alpha}(\tilde{\alpha}k_\gamma R')k_l(R',R'')j_{l_\beta}(\tilde{\beta}k_\gamma R'')f_{J_il_i}(R'')dR'dR''\ , \tag{56}$$

where $k_l(R',R'')$ has been defined in Eq. (35) of LKT. The explicit definitions of the various coefficients in Eqs. (55) and (56), specific for the different interaction types, are as follows:

(i) Type b

$$\mu_x=\mu_{bx},\quad\tilde{\alpha}=\tilde{\beta}=\lambda_{bx},\quad U_x=V_x=E_x^b\ . \tag{57}$$

(ii) Type c

$$\mu_x=\mu_{cx},\quad\tilde{\alpha}=\tilde{\beta}=\lambda_{cx},\quad U_x=V_x=E_x^c\ . \tag{58}$$

(iii) Type a1

$$\mu_x=\mu_{ax},\quad\tilde{\alpha}=\omega'_{ax}+\lambda_{ax},\quad\tilde{\beta}=\omega''_{ax}+\lambda_{ax},\quad U_x=P_x^a,\quad V_x=Q_x^a\ . \tag{59}$$

(iv) Type a2

$$\mu_x=\mu_{ax},\quad\tilde{\alpha}=\omega''_{ax}+\lambda_{ax},\quad\tilde{\beta}=\omega'_{ax}+\lambda_{ax},\quad U_x=Q_x^a,\quad V_x=P_x^a\ . \tag{60}$$

The quantities $(\mu_{bx},\mu_{cx},\mu_{ax})$, $(\lambda_{bx},\lambda_{cx},\lambda_{ax})$, and $(\omega'_{ax},\omega''_{ax})$ are defined, respectively, in Eqs. (61), (67), and (48), in Eqs. (62), (68), and (51), and in Eqs. (49) and (50) of KLT. The definitions of E_x^b, E_x^c, P_x^a, and Q_x^a have been listed in Eqs. (40)–(42) of Sec. II E.

For magnetic multipoles ($\sigma=1$), the direct terms are

$$Z_A\tilde{X}^{\,b}_0=a(J_il_iJ_fl_f;LS)C(l_iLl_f;1-10)i^{L+1}\sqrt{2\pi l_i(l_i+1)(2L+1)}\mu\left[-\frac{Z_Ae\hbar}{N_Am_nc}\right]\tilde{I}^{\,b}_0\exp(-\mu_{b0}k_\gamma^2)\ , \tag{61}$$

$$Z_B\tilde{X}^{\,c}_0=a(J_il_iJ_fl_f;LS)C(l_iLl_f;1-10)i^{L+1}\sqrt{2\pi l_i(l_i+1)(2L+1)}\mu\left[\frac{Z_Be\hbar}{N_Bm_nc}\right]\tilde{I}^{\,c}_0\exp(-\mu_{c0}k_\gamma^2)\ , \tag{62}$$

where the radial integral $\tilde{I}^{\,b}_0$ is[22]

$$\tilde{I}^{\,b}_0=\int f_{J_fl_f}(R')\frac{j_L(\gamma_bk_\gamma R')}{R'}f_{J_il_i}(R')dR'\ . \tag{63}$$

Again the radial integral $\tilde{I}^{\,c}_0$ can be similarly defined with γ_c replacing γ_b in Eq. (63). All the exchange terms are, quite interestingly, identical to those listed in Eqs. (55) and (56) with the same coefficients as in Eqs. (57)–(60).

Finally, we can express the bremsstrahlung triple cross section of Eq. (14) in multipoles in terms of the equation

$$\sum_{\mu,M_{S_i}} |\langle \phi^{(-)}_{SM_{S_f}} | \tilde{H}_e(\mathbf{k}_\gamma, \boldsymbol{\varepsilon}^*_\mu) | \phi^{(+)}_{SM_{S_i}} \rangle|^2$$

$$= \frac{1}{F^2_{\text{c.m.}}} \sum_\nu [1+(-1)^{L+L'-\lambda+\sigma+\sigma'}](-1)^{J_f-J_i-J_i'+G-L+L'-l_i'+k+J+\mu}$$

$$\times (2F+1)(2G+1)(2J_f+1)(2J_f'+1)\sqrt{(2J_i+1)(2J_i'+1)(2l_f+1)(2l_f'+1)}$$

$$\times X^\sigma_L(J_i l_i J_f l_f) X^{\sigma'*}_{L'}(J_i' l_i' J_f' l_f') W(l_i J_i F L; S J_f) W(l_i' J_i' G L'; S J_f') W(F L G L'; S\lambda) W(J_f l_f J_f' l_f'; S k)$$

$$\times \begin{Bmatrix} l_i & l_i' & J \\ J_f & J_f' & k \\ F & G & \lambda \end{Bmatrix} C(l_i l_i' J; 000) C(l_f l_f' k; 000) C(LL'\lambda; -\mu\mu 0) [Y_k(\hat{\mathbf{k}}_f) \otimes Y_\lambda(\hat{\mathbf{R}}_\gamma)]^J_0 , \tag{64}$$

for $\mu=+1$ on the right-hand side. The symbol ν stands for a collection of quantum numbers which are being summed,

$$\nu \equiv \{\sigma,\sigma',(J_i,l_i),(J_i',l_i'),(J_f,l_f),(J_f',l_f'),(L,L'),(J,k,\lambda),(F,G)\} .$$

The Harvard-geometry double cross section $d^2\sigma/d\Omega_A d\Omega_B$ is obtained after integrating Eq. (14) over θ_γ and multiplying by a factor of 2 to account for the two possible coplanar configurations with $\phi_\gamma=0$ and $\phi_\gamma=\pi$, and another factor of 2 to account for the fact that, because of low-energy photon emission, the experimental arrangement of Ref. 10 cannot distinguish the counters into which α and ^{3}He particles enter.

G. Qualitative discussion

For bremsstrahlung emission, neither the initial nor the final state is bound. This renders the long-wavelength approximation inapplicable and the Siegert theorem cannot be applied. Philpott and Halderson,[22] who were the first to emphasize this point, have shown that this more stringent condition is not a hindrance to deriving closed expressions for the reduced matrix elements. Our direct electric- and magnetic-multipole radial integrals of Eqs. (54) and (63) are essentially what these authors have presented. The exchange terms are the direct consequences of explicit antisymmetrization in our formalism. In the present section, our discussion does not make any specific reference to whether the initial and final states are bound or not.

The usual selection rule for electric-and magnetic-multipole transitions are implied in the reduced matrix elements of Eqs. (51), (52), (55), (61), and (62).

$$l_i+l_f+L = \text{even} . \tag{65}$$

In the exchange terms, this selection rule emerges also if we reconsider the multipole expansion of the vector potential of the photon field of Eq. (24), which is effectively Eq. (44) with $\gamma_b=1$ and $\mathbf{R}'$ substituted by $\mathbf{r}_i$. The explicit dependence on the circular polarization μ appears in two places, the rotation matrix $\mathcal{D}^{L*}_{M\mu}(\hat{\mathbf{R}}_\gamma)$ and the factor μ^σ. The same rotation matrix appears in the transition matrix element of Eq. (48). Hence, the μ dependence of the factor μ^σ must be implicit in the direct and exchange terms of the reduced matrix element of Eq. (50). For electric multipoles ($\sigma=0$), the factor μ^σ remains unchanged when μ changes its sign from $+1$ to -1 or vice versa. By inspection, the direct terms of Eqs. (51) and (52) exhibit this property, and so do the exchange terms $\tilde{X}^{\text{type}}_x$ of Eq. (55), if

$$l_\alpha+l_\beta+L = \text{even} . \tag{66}$$

Combining this with the selection rules from the other Clebsch-Gordan coefficients in Eq. (55),

$$l_i+l_\beta+l = \text{even} , \tag{67}$$

$$l_f+l_\alpha+l = \text{even} , \tag{68}$$

we obtain the usual selection rule, Eq. (65). Therefore, both the direct and exchange terms obey the same selection rule, Eq. (65), as they should.

For magnetic multipoles ($\sigma=1$), the direct terms of Eqs. (61) and (62) obey the usual selection rule

$$l_i+l_f+L = \text{odd} . \tag{69}$$

The factor μ^σ undergoes a sign change when μ changes its sign. The direct terms of Eqs. (61) and (62) exhibit this property, and so do the exchange terms $\tilde{X}^{\text{type}}_x$ of Eq. (55) if

$$l_\alpha+l_\beta+L = \text{odd} . \tag{70}$$

Combining this with Eqs. (67) and (68), we obtain the usual selection rule, Eq. (69). Hence, the direct and exchange terms obey the same selection rule, Eq. (69), as they should.

In a system of two identical clusters not heavier than the α particles, additional parity selection rules are also implicit in the equations for the reduced matrix elements in Sec. II F. Hence, when

$$N_A=N_B, \quad Z_A=Z_B, \quad \alpha_A=\alpha_B , \tag{71}$$

we find that

$$\tilde{X}^{b}_{0}=-\tilde{X}^{c}_{0},\quad \tilde{X}^{b}_{x}=-\tilde{X}^{c}_{x},\quad \tilde{X}^{a1}_{x}=-\tilde{X}^{a2}_{x}\ , \tag{72}$$

for electric-odd and magnetic-even transitions. Although Eq. (50) has been derived specifically for the system $\alpha+{}^3$He, the pairwise occurrences of $(\tilde{X}^{b}_{0},\tilde{X}^{c}_{0})$, $(\tilde{X}^{b}_{x},\tilde{X}^{c}_{x})$, and $(\tilde{X}^{a1}_{x},\tilde{X}^{a2}_{x})$ also appear in any system of two identical clusters not heavier than the α particles. Therefore, the reduced matrix element vanishes identically for

$$\text{electric}-\text{odd } L,\quad \text{magnetic}-\text{even } L \tag{73}$$

transitions. We are confident that the same selection rules must be explicitly derivable by an extension of the microscopic formalism to heavier systems.

It is often cited[26] that the electric-dipole transition vanishes when the following relationship holds:

$$\frac{Z_A}{N_A}-\frac{Z_B}{N_B}=0\ , \tag{74}$$

i.e., when the center of mass coincides with the center of charge, which, for example, is the case for $\alpha+\alpha$ or $d+\alpha$. We have proven this statement in the preceding paragraph for a system of two identical clusters. But for nonidentical particles, this is not borne out by Eq. (50). We can be easily convinced of this by examining the direct terms. Given Eq. (74), the direct term $Z_A\tilde{X}^{b}_{0}+Z_B\tilde{X}^{c}_{0}$ [see Eqs. (51) and (52)] of an electric-dipole transition vanishes only if

$$\tilde{I}^{b}_{0}/(\gamma_b k_\gamma)\exp(-\mu_{b0}k_\gamma^2)$$

is equal to

$$\tilde{I}^{c}_{0}/(\gamma_c k_\gamma)\exp(-\mu_{c0}k_\gamma^2)\ .$$

This is obviously not true for nonidentical clusters. Any further cancellation between the direct and exchange terms can only be entirely accidental and, thus, is extremely unlikely. Therefore, for nonidentical clusters, Eq. (74) does not imply a vanishing of the electric-dipole transition. However, this is an opportune moment to remind ourselves that the condition of Eq. (74) leads to a vanishing electric-dipole transition only when the long-wavelength approximation is valid, i.e., if we can approximate $j_1(\gamma_b k_\gamma R')\approx\gamma_b k_\gamma R'$ and $j_1(\gamma_c k_\gamma R')\approx\gamma_c k_\gamma R'$. Then, $Z_A\tilde{X}^{b}_{0}+Z_B\tilde{X}^{c}_{0}$ to a very good approximation is zero for electric-dipole transition. We note here that when the long-wavelength approximation is valid, the exponential factors $\exp(-\mu_{b0}k_\gamma^2)$ and $\exp(-\mu_{c0}k_\gamma^2)$ are practically unities. In the same approximation, the $x=1$, 2, and 3 exchange terms vanish individually.

In a semimicroscopic calculation, e.g., ARGM of Ref. 11, we write the cluster wave function as

$$\hat{\phi}^{(+)}_{SM_{S_i}}=\phi_A\phi_B\left[\frac{1}{R}\sum_{J_i l_i}\sum_{M_i}[4\pi(2l_i+1)]^{1/2}\hat{f}_{J_i l_i}(R)C(l_i S J_i;0M_{S_i}M_i)\mathcal{Y}^{M_i}_{J_i l_i S}\right]\ , \tag{75}$$

and its bound-state counterpart without the antisymmetrization operator $\mathcal{A}$. Antisymmetrization and other many-body effects are implied in the modified radial functions $\hat{f}_{Jl}(R)$. For the EM transition matrix element, we retain only the direct terms of Eqs. (34) and (35). At first glance, these equations seem to represent two clusters approximated by two structureless point charges $Z_a e$ and $Z_b e$, of masses $N_a m_n$ and $N_b m_n$, respectively, separated by $\mathbf{R}'$. The physical interpretation of Eqs. (34) and (35) is apparently straightforward. The former is the transition amplitude of a photon-emission operator, describing a photon-field interacting with a point charge $Z_a e$ situated at $\gamma_b\mathbf{R}'=(N_B/N)\mathbf{R}'$ from the combined c.m. of the two clusters, while the latter corresponds to a photon-field interacting with a point charge $Z_b e$ situated at $\gamma_c\mathbf{R}'=(-N_A/N)\mathbf{R}'$ from the combined c.m. of the two clusters. This is illustrated in Fig. 2. The origin of the implicit coordinate system used is placed at the combined c.m. of the two clusters. These two transition amplitudes interfere. However, this seeming loss of many-body information is in fact overstated because we must keep in mind that the finite sizes and other many-body information are implicit in the derivation of the radial function and explicitly contained in the exponential prefactors of the integrals. In a model in which the clusters are assumed to be point particles, we have

$$\alpha_A\to\infty,\quad \alpha_B\to\infty\ . \tag{76}$$

In this limit, the exponential prefactors are unities and the direct terms of Eqs. (34) and (35) and their subsequent multipole expansions of Eqs. (51), (52), (61), and (62) in Eq. (50) come closest to the most familiar expressions of nuclear EM transitions. Even with the realistic values of α_A and α_B given in Eqs. (5) and (6), we have, for the exponential prefactors,

$$\mu_{b0}=0.44\ \text{fm}^2,\quad \mu_{c0}=0.53\ \text{fm}^2\ . \tag{77}$$

At a photon energy of, say, 7 MeV,

$$k_\gamma^2=0.001\,25\ \text{fm}^{-2}\ . \tag{78}$$

Therefore, for a very broad range of photon energy, the exponential prefactors of Eqs. (34) and (35) are essentially unities. Of course, our previous discussion on the selection rules, Eqs. (65) and (69), of the electric- and magnetic-multipoles transitions apply equally, in this context, to just the direct terms. The same goes for the extra parity selection rules, Eq. (73), for a system of two identical clusters and the applicability of the rule of Eq. (74) in the long-wavelength approximation.

Also in the context of ARGM, when either the initial or the final state is bound, the integrands of Eqs. (54) and (63) vanish rapidly for large R'. Then it is straightforward to discuss which range of the R' space contributes the most to the integrals. Such an easy interpretative possibility is not open to us in bremsstrahlung. The following crude argument supports the plausible interpretation that bremsstrahlung emission nevertheless occurs in a rather restricted region of R' space. The radial in-

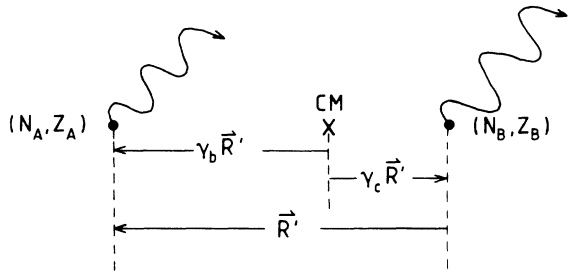

FIG. 2. The photon fields interacting with the α and ^{3}He clusters.

tegrands of Eqs. (54) and (63) contain terms that behave like $1/R'$ multiplied by a product of three oscillating functions. The oscillating integrand vanishes slowly for large R'. However, beyond a certain point, R'_N say, the integral from R'_N to infinity should vanish because the integrand is as often positive as it is negative. Of course, the value of R'_N, which is dependent on the three oscillating functions of the integrand, is difficult to pin-point. A reasonable guess would be that R'_N is not much greater than the radius of the nuclear interaction region. Thus, for the values of E_γ that we are concerned with here, $k_\gamma R'_N$ will be significantly smaller than unity and the relationship

$$\frac{\tilde{I}^{\,b}_0(L+1)}{\tilde{I}^{\,b}_0(L)} \propto k_\gamma R'_N \tag{79}$$

for both electric and magnetic transitions is expected to be on the whole valid.

The practical way of efficiently integrating the direct radial integrals, Eqs. (54) and (63), has been explained by Philpott and Halderson.[22] The crux of the matter is the slow convergence already mentioned. Such difficulty was first tackled successfully in the field of stripping to unbound states. The slow convergence was expedited most efficiently by the contour-integration method of Vincent and Fortune.[30] This integration procedure had been incorporated in the latest bremsstrahlung calculation[22,5,6] and in our present work. The exchange radial integrals of Eq. (56) do not require special handling because the function $k_l(R',R'')$ in the integrand decays exponentially.

III. RESULTS

The only available experimental bremsstrahlung result of this system was obtained by Frois *et al.*[10] at $E(^3\text{He})=7.4$ MeV with $\theta_{A,B}=37°$, i.e., $E_\gamma=2.32$ MeV. The bremsstrahlung double cross section $d^2\sigma/d\Omega_A d\Omega_B$ was measured to be 12.6 ± 3.4 μb/sr^2.

We tabulate in Table II the detailed results of our calculation at this energy and experimental arrangement. We have investigated the convergence behavior of the double cross section with respect to the maximum values of l_i and l_f used in the calculation. The multipoles we have included are $E1$, $E2$, and $M1$. All the results show convergence up to three significant figures for maximum $l_i=l_f=14$. We could achieve an even smoother convergence if we apply a Padé approximation to the intermediate results[31] [as a function of $l_{i,f}(\max)$]. As expected, $E1$ is the dominant transition. The $E2$ contribution seems an order of magnitude smaller, with the $M1$ contribution another order of magnitude smaller still. The $E2$ and $M1$ contributions interfere destructively with the $E1$ contribution. We have also ascertained that an $E3$ transition, albeit of another order of magnitude smaller than the $E2$, interferes constructively with the $E1$ transition. Of course, these interference characteristics would change when the detection angles $\theta_{A,B}$ change. The initial and final energies are 4.23 and 1.91 MeV, which are above and below the narrow $\frac{7}{2}^-$ resonance, respectively. Therefore, the $l_{i,f}=3$ partial waves are not expected to be of particular importance. The results in Table II are consistent with this view—the bulk of the final convergent value of the double cross section has been accounted for when $l_{i,f}(\max)=2$. It is clear from Table II that the cross section continues to oscillate significantly up to $l_{i,f}(\max)$ around 10. Our theoretical value for the double

TABLE II. The double cross section $d^2\sigma/d\Omega_A d\Omega_B$ (μb/sr^2) for $E(^3\text{He})=7.4$ MeV at $\theta_{A,B}=37°$.

	$d^2\sigma/d\Omega_A d\Omega_B$ (μb/sr^2)		
$l_{i,f}(\max)$	$E1$ (Padé approximation)	$E1+E2$	$E1+E2+M1$
1	1.18(1.18)	1.22	1.22
2	8.56(8.56)	7.43	7.42
3	8.97(9.00)	7.59	7.56
4	8.78(8.84)	7.61	7.59
5	8.72(8.71)	7.57	7.55
6	8.55(8.99)	7.45	7.42
7	8.48(6.96)	7.42	7.39
8	8.57(8.78)	7.46	7.44
9	8.65(8.58)	7.48	7.46
10	8.62(8.60)	7.48	7.45
11	8.56(8.59)	7.46	7.44
12	8.56(8.59)	7.46	7.44
13	8.58(8.59)	7.46	7.43
14	8.58(8.59)	7.45	7.43

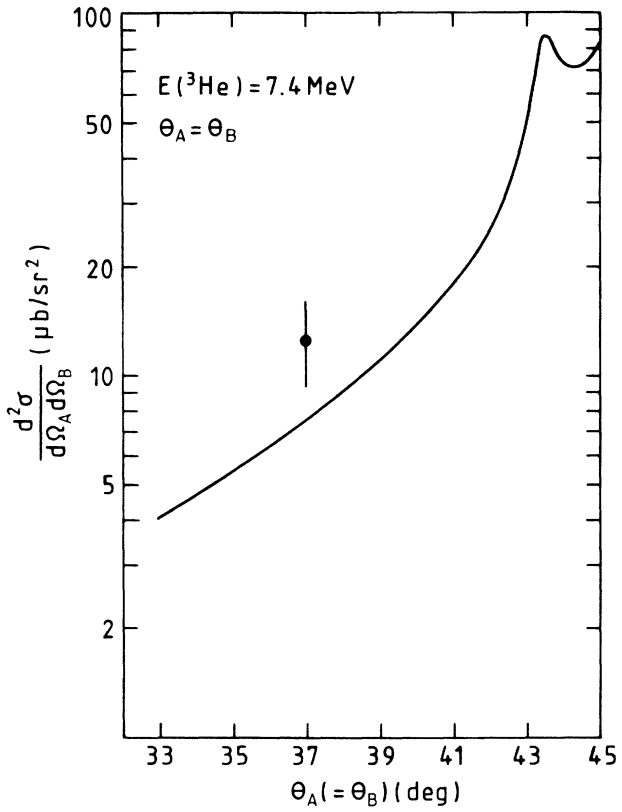

FIG. 3. The double cross section $d^2\sigma/d\Omega_A d\Omega_B$ (μb/sr^2) as a function of the polar angle $\theta_{A,B}$. The calculated results shown have not yet been corrected for finite polar-angle openings of the detectors.

cross section from Table II is 7.43 μb/sr^2. This is a value for infinite angular resolution. In order to compare with the experimental value measured with finite angular resolution, we shall make use of the calculated results discussed in the next paragraphs.

Throughout the rest of this section, we shall show results which have been calculated with $l_{i,f}(\max)=14$. Furthermore, we save computational time by not including the $M1$ transition. This negligible loss of accuracy is supported by the results in Table II.

Bremsstrahlung double cross sections have been calculated for the incident energy $E(^3\text{He})=7.4$ MeV, which is the energy used in the measurement of Frois *et al.*,[10] and a series of polar angles for the detectors from $\theta_a=\theta_B=33°-45°$. The results are plotted in Fig. 3, which shows a rising trend as a function of $\theta_{A,B}$. This qualitative feature was also obtained from a macroscopic calculation.[10] At $\theta_A=\theta_B=43.5°$, E_f is equal to 2.98 MeV, which corresponds to the energy of the $\frac{7}{2}^-$ resonance. At this angle, we clearly see a peak superimposed on the rising trend. The position and the width of this peak are evidence for identifying it as the $\frac{7}{2}^-$ resonance. The single measurement made by Frois *et al.*[10] at $\theta_{A,B}=37°$ is also drawn in Fig. 3. We make use of our explicit calculations for the cases of $\theta_{A,B}=35°$, 37°, and 39° and the detector efficiency diagram in Fig. 6 of Ref. 10 to estimate the finite angular-resolution correction to

TABLE III. The double cross section $d^2\sigma/d\Omega_A d\Omega_B$ (μb/sr^2) for $E(^3\text{He})=7.4$ MeV at $\theta_{A,B}=43.5°$.

$l_{i,f}(\max)$	$d^2\sigma/d\Omega_A d\Omega_B$ (μb/sr^2) $E1+E2$
1	4.9
2	38.8
3	56.9
4	86.5
5	86.8
6	86.9
7	86.9
8	86.7
9	86.6
10	86.8
11	86.9
12	86.8
13	86.7
14	86.7

our calculated value of 7.43 μb/sr^2 for the double cross section at $\theta_{A,B}=37°$. Our polar-angle corrected value is 8.30 μb/sr^2, which is slightly less than the measured value of 12.6±3.4 μb/sr^2 of Ref. 10, but does not constitute a reason for alarm. A more extensive comparison would have been helpful if there were more experimental values available. Suspicion of imperfection in the measurements of Ref. 10 has been expressed by BD (Ref. 5) and Langanke.[6]

In Table III we tabulate the double cross section as a function of $l_{i,f}(\max)$, with $\theta_{A,B}=43.5°$ and $E(^3\text{He})=7.4$ MeV, i.e., E_f is at the $\frac{7}{2}^-$ resonance energy of 2.98 MeV. For the important $E1$ transitions, the contributions of the couplings from $l_i=2$ and 4 to $l_f=3$ are certainly substantial, but we see that over 40% of the cross section

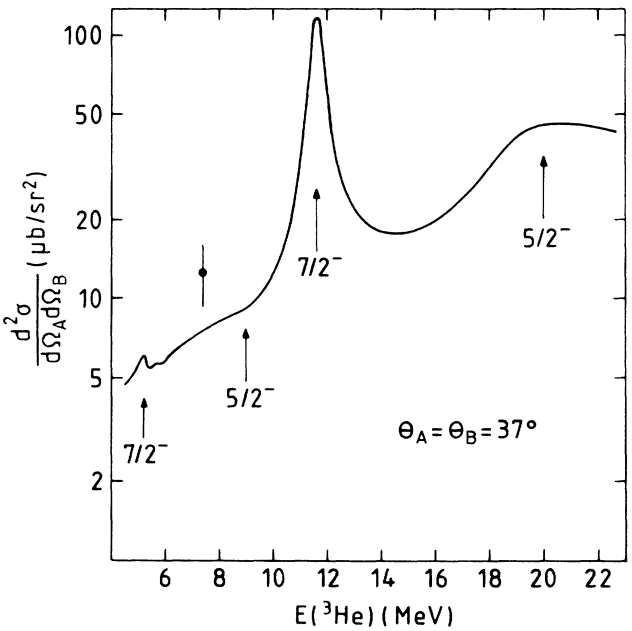

FIG. 4. The double cross section $d^2\sigma/d\Omega_A d\Omega_B$ (μb/sr^2) at $\theta_{A,B}=37°$ as a function of $E(^3\text{He})$.

could be accounted for if we set $l_{i,f}(\max)=2$. We have also taken note that, for $\theta_{A,B}\neq 43.5°$, the contributions from $l_f=3$ diminish drastically as expected.

We plot in Fig. 4 our calculated double cross sections for $\theta_{A,B}=37°$, spanning the energy range from $E(^3\text{He})=5$–22 MeV. The locations of the $\frac{7}{2}^-$ and $\frac{5}{2}^-$ resonances are indicated. The two lower positions of the resonances at $E(^3\text{He})=5.2$ and 9.0 MeV correspond to resonances occurring in the initial channel, and the upper two at $E(^3\text{He})=11.6$ and 20.0 MeV correspond to the resonances in the final channel. The most notable feature is the contrast between the same two resonances in the initial and final channels. A probable explanation for this is the penetration of the Coulomb barrier. A crude estimate of the barrier height is 1.84 MeV, which is the Coulomb potential when α and ^{3}He are separated by the sum of their rms radii[15] of 3.13 fm. When bremsstrahlung is emitted from the $\frac{7}{2}^-$(2.98 MeV) and $\frac{5}{2}^-$(5.14 MeV) resonances in the initial channel with $E(^3\text{He})=5.2$ and 9.0 MeV, respectively, the energies in the final channel E_f are 1.34 MeV and 2.32 MeV, respectively. For the former, the final-state energy is below the Coulomb barrier, which, together with the centrifugal barrier, effectively prevents substantial overlap between initial and final states. For the latter, the final-state energy is somewhat above our crude estimate of the barrier. However, this resonance has a width $\Gamma=1.2$ MeV. These might be the reasons for the relative flatness in the double cross section below $E(^3\text{He})=10$ MeV. In the case where the resonances occur in the final state, the initial-state energies are well above the barrier. Here the pronounced shapes of the two resonances are clearly identifiable in the double cross section. A clearer picture of the role played by the Coulomb barrier would emerge if we bring in the semimicroscopic ARGM formalism[11] and examine the behavior of the approximated radial function $\hat{f}_{Jl}(R)$. In all the calculations done in this range of energy, the absolute magnitude of the ratio of the exchange to direct contributions to the reduced matrix element decreases to an order of magnitude 10^{-3} for $l_{i,f}=6$ or 7.

For kinematical reasons, the positions of the $\frac{7}{2}^-$ and $\frac{5}{2}^-$ resonances in the spectrum of Fig. 4 change as a function of the polar angles $\theta_{A,B}$. Such a manipulation could be advantageous. In Fig. 4, the $\frac{5}{2}^-$ resonance at $E(^3\text{He})=9.0$ MeV is rather swamped by the $\frac{7}{2}^-$ resonance at $E(^3\text{He})=11.6$ MeV. By changing $\theta_{A,B}$, we can change the separation between these two resonances, causing them either to be further apart for easier analysis, or to overlap strongly to enhance (or suppress) the bremsstrahlung emission. In Fig. 5 we display our calculated result of the double cross section for $\theta_{A,B}=35°$, 37°, and 39°. Because of different kinematical conditions, the same $\frac{7}{2}^-$ resonance in the final channel appears at $E(^3\text{He})=13.3$, 11.6, and 10.1 MeV, respectively. For $\theta_{A,B}=35°$, the $\frac{7}{2}^-$ resonance in the final channel is sufficiently far away from the $\frac{5}{2}^-$ resonance in the initial channel that the latter gives rise to a structure in the spectrum that was not visible at $\theta_{A,B}=37°$ (see the inset of Fig. 5).

We show in Fig. 6 the triple cross section

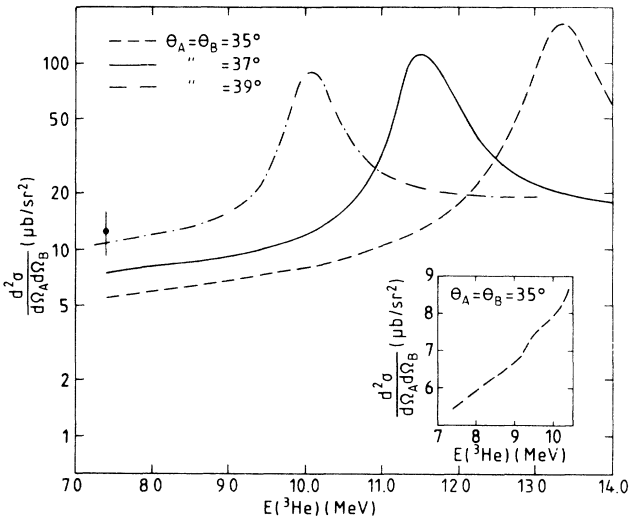

FIG. 5. The double cross section $d^2\sigma/d\Omega_A d\Omega_B$ (μb/sr^2) as a function of $E(^3\text{He})$, for $\theta_{A,B}=35°$, 37°, and 39°.

$d^3\sigma/d\Omega_A d\Omega_B d\theta_\gamma$ as a function of θ_γ for two energies $E_f=2.98$ and 2.23 MeV, i.e., at the $\frac{7}{2}^-$ resonance and off resonance. For comparison, we plot also the cross sections for pure electric-dipole transitions. The general features of the dipole triple cross section at resonance can be understood rather easily as follows. From our detailed

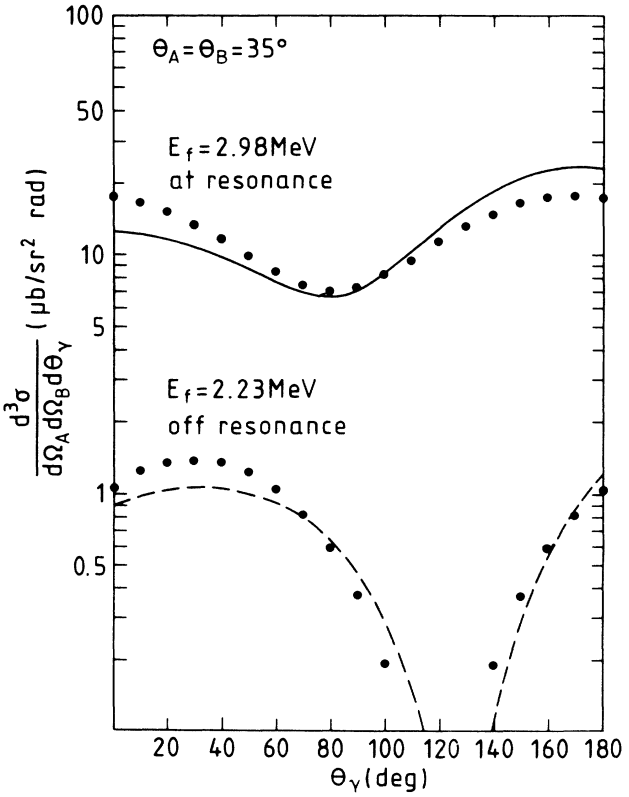

FIG. 6. The triple cross section $d^3\sigma/d\Omega_A d\Omega_B d\theta_\gamma$ (μb/sr^2 rad) as a function of θ_γ, for $E_f=2.98$ MeV (at resonance), and $E_f=2.23$ MeV (off resonance). The cases of pure electric dipole transition (● ● ●) are also plotted for comparison.

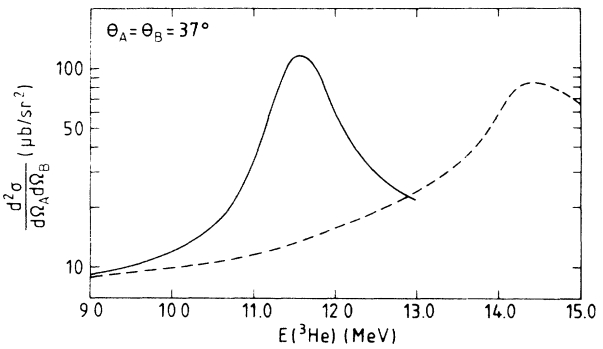

FIG. 7. Comparison of $d^2\sigma/d\Omega_A d\Omega_B$ (μb/sr^2) calculated with the parameters of the present work (——) and LKT (— — —).

numerical results, we note that at resonance the $\frac{9}{2}^+ \rightarrow \frac{7}{2}^-$ transition dominates. Hence, we can approximate the sum in Eq. (64) by restricting it to $l_i = l_i' = 4$ and $l_f = l_f' = 3$. Furthermore, for electric-dipole transition, the expression in Eq. (64) is nonvanishing only if $L + L' + \lambda =$ even, i.e., $\lambda = 0$ and 2. Of the components of the spherical harmonics $Y_\lambda^m(\hat{\mathbf{R}}_\gamma)$ involved, the term $Y_0^0(\hat{\mathbf{R}}_\gamma)$ is a constant. The terms $Y_2^2(\hat{\mathbf{R}}_\gamma)$, $Y_2^0(\hat{\mathbf{R}}_\gamma)$, and $Y_2^{-2}(\hat{\mathbf{R}}_\gamma)$ are symmetrical about $\theta_\gamma = \pi/2$. Together they account for the overall shape of the triple cross section in Fig. 6. The slight asymmetry about $\theta_\gamma = \pi/2$ is due to the presence of the $Y_2^1(\hat{\mathbf{R}}_\gamma)$ and $Y_2^{-1}(\hat{\mathbf{R}}_\gamma)$ terms. However, they vanish for $\theta_\gamma = 0$ and π. Hence, the triple cross sections are equal at $\theta_\gamma = 0$ and π. In fact, after subtracting an isotropic part from the angular distribution, the result has the point of symmetry near $\theta_\gamma = 80°$, but the magnitude is largely proportional to $Y_2^0(\hat{\mathbf{R}}_\gamma)$. Clearly, when $E2$ transition is included, the angular distribution is further distorted from the symmetry about $\theta_\gamma = \pi/2$. When we move away from the resonance, contributions from other transitions destroy any simple understanding of even the dipole angular distribution.

Finally, we illustrate with Fig. 7 the importance of reproducing accurately the experimental phase shifts if we want to compare theoretical bremsstrahlung cross sections with empirical results, especially in the vicinity of sharp resonances. The solid line is produced by the RGM wave functions using the potential parameters of the present work, discussed in Sec. II B, which reproduce the $\frac{7}{2}^-$ and $\frac{5}{2}^-$ empirical phase shifts. The dashed line represents results from using the potential parameters in LKT. The peaks from these calculations correspond to their predictions of the $\frac{7}{2}^-$ resonance.

IV. CONCLUSION

We have investigated the bremsstrahlung emission in ^{3}He+α collision by using single-channel RGM wave functions to describe the seven-nucleon system. The bremsstrahlung problem has been formulated as the EM transition between nuclear states with a translationally invariant photon-emission operator. The center-of-mass motion is eliminated rigorously from the transition amplitude and, hence, its multipole expansion. Such a strict elimination, given the general analytic nature of our RGM wave function, hinges on the use of the transverse gauge condition for the photon-emission operator. Closed expressions are derived for the direct and exchange parts of the reduced matrix element without invoking the often used long-wavelength approximation. Since no reference is made to whether the nuclear states involved are bound or not, our expressions for the EM transition amplitude are valid for a whole range of EM transitions: (a) EM form factor—a transition between bound states with virtual photon; (b) the usual transition between bound states with the emission of a real photon; (c) radiative capture reaction—an EM transition between a scattering and a bound state with the emission of a real photon; (d) bremsstrahlung emission—an EM transition between scattering states with the emission of a real photon. All the usual parity selection rules for electric and magnetic transitions are implied in our expressions. For the case of the nuclear system made up of two identical clusters, the E (odd L) and M (even L) transitions are shown to be not allowed. We have also discussed the qualification to the usual statement that $E(1)$ transitions vanish for cases in which the center of mass coincides with the center of charge—this is true only in the long-wavelength approximation.

In order to compare our result with experimental value, we have fine-tuned our previous potential parameters[8] to reproduce the energy positions of the important $\frac{7}{2}^-$ and $\frac{5}{2}^-$ resonances. The calculated bremsstrahlung double cross section, $d^2\sigma/d\Omega_A d\Omega_B$, after making polar-angle correction, is 8.30 μb/sr^2, which is slightly below the measured value[10] of 12.6±3.4 μb/sr^2. Our results show the relative unimportance of the $E3$ and $M1$ multipoles, and presumably all the higher multipoles. They also show convergence with respect to $l_{i,f}$ by our examination with $l_{i,f}(\max)$ up to 14. This convergence can be further expedited by using the Padé approximation. In our theoretical study, the important $\frac{7}{2}^-$ and $\frac{5}{2}^-$ resonances are accounted for under various experimental conditions.

From the success of our bremsstrahlung investigation, we are encouraged to feel that a few follow-up problems would be interesting to explore. Up to now we have seen that the ARGM formalism[11] could reproduce rather accurately the RGM results in form factors and radiative capture transitions, and therefore we presume that this might be true in bremsstrahlung too. But it would be interesting to test it again in this situation where many more transition amplitudes interfere with each other.

It is well-established that the description of the seven-nucleon system can be improved by introducing specific distortion[9] to the resonating-group wave function. It would be interesting to see how the bremsstrahlung results would be affected.

On the other hand, there are systems in which distortion hardly plays a role, e.g., in $p+\alpha$ collision, due to the extreme stability of the α particle. This is a particularly good candidate for further bremsstrahlung investigation because there are more experimental data available.[32] The appropriate reduced matrix element in this case

different combination of exchange terms in Eq. (50).

Macroscopic models in which scattering states are generated for two structureless particles are always much simpler to handle. Some have already been mentioned in Sec. I. In these models, only the direct terms in the reduced matrix element of Eq. (50) would appear. The question of their accuracies would be directly probed by a comparison with the unabridged calculation with Eq. (50).

In conclusion, we feel that we have made a useful contribution to the discussion on EM transition in a many-body system, in the elimination of the c.m. motion and in the avoidance of the long-wavelength approximation. Our bremsstrahlung calculation confirms the conclusions in our previous EM studies that our single-channel RGM wave functions on the whole describe the seven-nucleon system quite accurately. New avenues of exploration have opened up in related EM transitions which we intend to follow up.

ACKNOWLEDGMENTS

We thank D. Baye, D. Halderson, K. Langanke, R. Lipperheide, and R. J. Philpott for valuable discussions. Part of the work discussed in this publication was done with the help of MACSYMA (Symbolics, Inc). This research was supported in part by the U.S. Department of Energy under Contract No. DOE/DE-AC02-79-ER10364 and by the Supercomputer Institute of the University of Minnesota.

APPENDIX: ELIMINATION OF THE c.m. MOTION FROM THE TRANSITION AMPLITUDE OF THE SPIN-DEPENDENT PHOTON-EMISSION OPERATOR

From Ref. 20, the spin-dependent part of the photon-emission operator in independent-particle coordinates is

$$H_e(\mathbf{k}_\gamma,\boldsymbol{\varepsilon}_\mu^*)=-\sum_{i=1}^{N}\frac{e\hbar}{2m_nc}g_s(i)\mathbf{s}^*(i)\cdot\nabla_{\mathbf{r}_i}\times\boldsymbol{\varepsilon}_\mu^*\exp(-i\mathbf{k}_\gamma\cdot\mathbf{r}_i)\ , \tag{A1}$$

where $g_s=5.585$ or -3.826 for a proton or a neutron, respectively. The manipulation of the vector potential $\boldsymbol{\varepsilon}_\mu^*\exp(-i\mathbf{k}_\gamma\cdot\mathbf{r}_i)$ proceeds in the following way,

$$\nabla_{\mathbf{r}_i}\times\boldsymbol{\varepsilon}_\mu^*\exp(-i\mathbf{k}_\gamma\cdot\mathbf{r}_i)=-i\mathbf{k}\times\boldsymbol{\varepsilon}_\mu^*\exp(-i\mathbf{k}_\gamma\cdot\mathbf{r}_i) \tag{A2}$$

$$=[-i\mathbf{k}\times\boldsymbol{\varepsilon}_\mu^*\exp(-i\mathbf{k}_\gamma\cdot\boldsymbol{\rho}_i)]\exp(-i\mathbf{k}_\gamma\cdot\mathbf{R}_{\text{c.m.}}) \tag{A3}$$

$$=[\nabla_{\boldsymbol{\rho}_i}\times\boldsymbol{\varepsilon}_\mu^*\exp(-i\mathbf{k}_\gamma\cdot\boldsymbol{\rho}_i)]\exp(-i\mathbf{k}_\gamma\cdot\mathbf{R}_{\text{c.m.}})\ . \tag{A4}$$

The step from Eq. (A2) to Eq. (A3) is facilitated by the substitution of the inverse of Eq. (20). Substituting Eq. (A4) into the sum in Eq. (A1), we obtain easily

$$H_e(\mathbf{k}_\gamma,\boldsymbol{\varepsilon}_\mu^*)=\left[-\sum_{i=1}^{N}\frac{e\hbar}{2m_nc}g_s(i)\mathbf{s}^*(i)\cdot\nabla_{\boldsymbol{\rho}_i}\times\boldsymbol{\varepsilon}_\mu^*\exp(-i\mathbf{k}_\gamma\cdot\boldsymbol{\rho}_i)\right]\exp(-i\mathbf{k}_\gamma\cdot\mathbf{R}_{\text{c.m.}})$$

$$=\tilde{H}_e(\mathbf{k}_\gamma,\boldsymbol{\varepsilon}_\mu^*)\exp(-i\mathbf{k}_\gamma\cdot\mathbf{R}_{\text{c.m.}})\ . \tag{A5}$$

The operator $\tilde{H}_e(\mathbf{k}_\gamma,\boldsymbol{\varepsilon}_\mu^*)$ is expressed in terms of the translationally invariant coordinates of the nucleons $\boldsymbol{\rho}_i$ and is our desired spin-dependent translationally invariant photon-emission operator. We note that it has exactly the same form as the first term of Eq. (25) for the spin-independent counterpart. We have proven in Sec. II D that with our RGM wave function, only the first term of Eq. (25) contributes towards the transition amplitude. Therefore, Eq. (29) is true for the entire photon-emission operator,

$$\langle\phi^{(-)}_{SM_{S_f}}|\tilde{H}_e|\phi^{(+)}_{SM_{S_i}}\rangle=\frac{\langle\psi^{(-)}_{SM_{S_f}}|H_e|\psi^{(+)}_{SM_{S_i}}\rangle}{F_{\text{c.m.}}}$$

with

$$H_e(\mathbf{k}_\gamma,\boldsymbol{\varepsilon}_\mu^*)=-\sum_{i=1}^{N}\left[\frac{e}{m_nc}g_l(i)\boldsymbol{\varepsilon}_\mu^*\exp(-i\mathbf{k}_\gamma\cdot\mathbf{r}_i)\cdot\mathbf{p}_i^*+\frac{e\hbar}{2m_nc}g_s(i)\mathbf{s}^*(i)\cdot\nabla_{\mathbf{r}_i}\times\boldsymbol{\varepsilon}_\mu^*\exp(-i\mathbf{k}_\gamma\cdot\mathbf{r}_i)\right]\ , \tag{A6}$$

$$\tilde{H}_e(\mathbf{k}_\gamma,\boldsymbol{\varepsilon}_\mu^*)=-\sum_{i=1}^{N}\left[\frac{e}{m_nc}g_l(i)\boldsymbol{\varepsilon}_\mu^*\exp(-i\mathbf{k}_\gamma\cdot\boldsymbol{\rho}_i)\cdot\mathbf{P}_i^*+\frac{e\hbar}{2m_nc}g_s(i)\mathbf{s}^*(i)\cdot\nabla_{\boldsymbol{\rho}_i}\times\boldsymbol{\varepsilon}_\mu^*\exp(-i\mathbf{k}_\gamma\cdot\boldsymbol{\rho}_i)\right]\ . \tag{A7}$$

[1]K. Wildermuth and Y. C. Tang, *A Unified Theory of the Nucleus* (Vieweg, Braunschweig, Germany, 1977).
[2]F. Ajzenberg-Selove, Nucl. Phys. **A490**, 1 (1988).
[3]S. Saito, Prog. Theor. Phys. **41**, 705 (1969); K. Kato, S. Okabe, and Y. Abe, Prog. Theor. Phys. **68**, 1794 (1982).
[4]R. L. McGrath, D. Abriola, J. Karp, T. Renn, and Y. Zhu, Phys. Rev. C **24**, 2374 (1981); V. Metag, A. Lazzarini, K. Lesko, and R. Vandenbosch, Phys. Rev. C **25**, 1486 (1982).

[5]D. Baye and P. Descouvemont, Nucl. Phys. **A443**, 302 (1985).
[6]K. Langanke, Phys. Lett. B **174**, 27 (1986).
[7]H. Kanada, Q. K. K. Liu, and Y. C. Tang, Phys. Rev. C **22**, 813 (1980).
[8]Q. K. K. Liu, H. Kanada, and Y. C. Tang, Phys. Rev. C **23**, 645 (1981).
[9]H. Walliser, Q. K. K. Liu, H. Kanada, and Y. C. Tang, Phys. Rev. C **28**, 57 (1983); H. Walliser, H. Kanada, and Y. C. Tang, Nucl. Phys. **A419**, 133 (1984).
[10]B. Frois, J. Birchall, C. R. Lamontagne, U. von Moellendorff, R. Roy, and R. J. Slobodrian, Phys. Rev. C **8**, 2132 (1973).
[11]Q. K. K. Liu, H. Kanada, and Y. C. Tang, Z. Phys. **A303**, 253 (1981); H. Walliser and T. Fliessbach, Phys. Rev. C **31**, 2242 (1985); Q. K. K. Liu, H. Kanada, and Y. C. Tang, Phys. Rev. C **33**, 1561 (1986).
[12]B. Buck, H. Friedrich, and C. Wheatley, Nucl. Phys. **A275**, 246 (1977).
[13]D. Baye, Phys. Rev. Lett. **58**, 2738 (1987).
[14]R. D. Furber, R. E. Brown, G. L. Peterson, D. R. Thompson, and Y. C. Tang, Phys. Rev. C **25**, 23 (1982).
[15]J. A. Koepke, R. E. Brown, Y. C. Tang, and D. R. Thompson, Phys. Rev. C **9**, 823 (1974).
[16]M. E. Rose, *Elementary Theory of Angular Momentum* (Wiley, New York, 1957).
[17]W. Sünkel and K. Wildermuth, Phys. Lett. **41B**, 439 (1972); Y. C. Tang, M. LeMere, and D. R. Thompson, Phys. Rep. **47**, 167 (1978).
[18]G. G. Ohlson, Nucl. Instrum Methods **37**, 240 (1965); H. Fuchs, *ibid.* **200**, 361 (1982); R. J. deMeijer and R. Kamermans, Rev. Mod. Phys. **57**, 147 (1985).
[19]D. Drechsel and L. C. Maximon, Ann. Phys. **49**, 403 (1968).
[20]H. J. Rose and D. M. Brink, Rev. Mod. Phys. **39**, 306 (1967).
[21]S. A. Moszkowski, in *Alpha-, Beta-, and Gamma-Ray Spectroscopy,* edited by K. Siegbahn (North-Holland, Amsterdam, 1966), p. 863.
[22]R. J. Philpott and D. Halderson, Nucl. Phys. **A375**, 169 (1982).
[23]L. J. Tassie and F. C. Barker, Phys. Rev. **111**, 940 (1958); T. deForest and J. D. Walecka, Adv. Phys. **15**, 1 (1966).
[24]T. Kajino, T. Matsuse, and A. Arima, Nucl. Phys. **A413**, 323 (1984).
[25]D. Baye and P. Descouvemont, Nucl. Phys. **A407**, 77 (1983).
[26]A. deShalit and H. Feshbach, *Theoretical Nuclear Physics* (John Wiley and Son, New York, 1974), Vol. 1, p. 706.
[27]MACSYMA (Version Ten) (MIT, Cambridge, 1983).
[28]D. M. Brink and G. R. Satchler, *Angular Momentum* (Oxford University Press, Oxford, 1968), p. 69.
[29]*Handbook of Mathematical Functions,* Natl. Bur. Stand. Appl. Math. Ser. No. 55, edited by M. Abramowitz and I. A. Stegun (U.S. GPO, Washington, D.C., 1972).
[30]C. M. Vincent and H. T. Fortune, Phys. Rev. C **2**, 782 (1970); R. Huby, in *Cooperative Phenomena,* edited by H. Haken and M. Wagner (Springer-Verlag, West Germany, 1974), p. 326.
[31]G. A. Baker, Jr., *Essentials of Padé Approximants* (Academic, New York, 1975), p. 74.
[32]W. Wölfli, J. Hall, and R. Müller, Phys. Rev. Lett. **27**, 271 (1971).